

Generative Models Improve Radiomics Reproducibility in Low Dose CTs: A Simulation Study

Junhua Chen¹, Chong Zhang¹, Alberto Traverso¹, Ivan Zhovannik^{1,2}, Andre Dekker¹, Leonard Wee^{1,3} and Inigo Bermejo^{1,3}

¹ Department of Radiation Oncology (MAASTRO), GROW School for Oncology and Developmental Biology, Maastricht University Medical Centre+, Maastricht, 6229 ET, Netherlands

² Department of Radiation Oncology, Radboud Institute for Health Sciences, Radboud University Medical Center, Nijmegen, 6525 GA, Netherlands

³ equally senior author

E-mail: Junhua.chen@maastro.nl

Received 30/04/2021.

Accepted for publication XXXXXX

Published XXXXXX

Abstract

Radiomics is an active area of research in medical image analysis, the low reproducibility of radiomics has limited its applicability to clinical practice. This issue is especially prominent when radiomic features are calculated from noisy images, such as low dose computed tomography (CT) scans. In this article, we investigate the possibility of improving the reproducibility of radiomic features calculated on noisy CTs by using generative models for denoising. One traditional denoising method – non-local means – and two generative models – encoder-decoder networks (EDN) and conditional generative adversarial networks (CGANs) – were selected as the test models. We added noise to the sinograms of full dose CTs to mimic low dose CTs with two different levels of noise: low-noise CT and high-noise CT. Models were trained on high-noise CTs and used to denoise low-noise CTs without re-training. We also test the performance of our model in real data, using dataset of same-day repeat low dose CTs to assess the reproducibility of radiomic features in denoised images. The EDN and the CGAN improved the concordance correlation coefficients (CCC) of radiomic features for low-noise images from 0.87 to 0.92 and for high-noise images from 0.68 to 0.92 respectively. Moreover, the EDN and the CGAN improved the test-retest reliability of radiomic features (mean CCC increased from 0.89 to 0.94) based on real low dose CTs. The results show that denoising using EDN and CGANs can improve the reproducibility of radiomic features calculated on noisy CTs. Moreover, images with different noise levels can be denoised to improve the reproducibility using these models without re-training, as long as the noise intensity is equal or lower than that in high-noise CTs. To the authors' knowledge, this is the first effort to improve the reproducibility of radiomic features calculated on low dose CT scans by using generative models.

Keywords: Radiomics; Reproducibility; Computed Tomography; Denoising; Generative Models

1. Introduction

Radiomics is currently an active area of research in medical image analysis. It comprises the automated extraction of (either hand-crafted or deep-learning) quantitative image metrics known as “features”, in the hope of improving diagnostic, prognostic, and predictive accuracy[1]. One of the biggest advantages of Radiomics by comparing with deep features is higher interpretability for human.

Radiomics has shown potential for clinical-decision support in oncology in a range of cancers (lung cancers, [2] head and neck cancer, [3] rectal cancer [4]) and using most common clinical imaging modalities such as computed tomography (CT), [3][5] magnetic resonance imaging (MRI), [6] and positron emission tomography (PET) [7]. Radiomics has attracted increased attention from researchers following the seminal article by Aerts et al. [7] published in 2014, especially for experts from medical physics domain. In spite of significant progress made during recent years by hundreds of researchers, there are still important barriers that prevent the widespread implementation of radiomics in clinical settings. One important issue is the low repeatability and reproducibility of radiomic features [8]. Repeatability mainly refers to features that remain the same when imaged multiple times in the same subject. The repeatability of radiomic features is assessed in test-retest analyses [9] and interobserver variability for tumor contouring [10]. On the other hand, reproducibility of radiomics refers to stability of features when at least one condition (equipment, software, acquisition settings, etc.) is changed. The reproducibility of radiomics features is assessed using different acquisition protocols [11], different radiation dose in CT scanning [12], etc.

One potential source of non-reproducibility or limited generalizability in radiomics that demands more attention is the effect of noise in images. Due to the long term risk posed by low levels of ionizing radiation exposure, low dose CTs have become more popular (ALARA principle [16]) especially for screening and monitoring of populations at risk. Therefore, researchers have started to calculate radiomic features based on low dose CTs. As a trade-off of for low radiation exposure in low dose CT imaging, higher noise is present in these images. This noise decreases the image texture. [13] As reported in [11], changes in radiation dose limit the reproducibility of radiomic features and features from low dose CT images have lower reproducibility. [12] More specifically, image noise has been shown to impact the reproducibility of radiomic features negatively when signal to noise ratio (SNR) falls below 50 dB [5]. However, the results show that some radiomics features are robust to low-pass filtering. Improving the reproducibility of radiomics from low dose CTs is therefore a timely and potentially impactful research topic.

To the best of the authors’ knowledge, currently there are no published detailed analyses how to improve the robustness of radiomic features based on low dose CT. One potential solution worth exploring for improving the reproducibility of radiomics based on low dose CT is denoising the images before extracting radiomic features [12].

For medical image denoising, many effective procedures have been proposed to improve low dose CTs’ image quality and recover texture information, such as building a more sophisticated imaging platform[14], denoising in the CT sinogram domain[15], denoising in the CT image domain, etc. The most convenient and popular denoising methods for low dose CT images operate in the CT image domain because hardware and sonograms of CTs are hard to access for most researchers [22]. Generally speaking, higher image quality can introduce higher reproducibility of radiomics, therefore, denoising seems a useful pre-processing step for improving radiomics reproducibility from low dose CT.

Hundreds of articles describing image denoising techniques have been published so far, as shown in reviews [17][18]. They can be divided into two main categories: traditional denoising methods and deep learning-based methods. Traditional denoising methods [19] have known limitations such as loss of details in images. Following the advent of deep learning, a series of publications have showed that generative model based methods can outperform traditional methods in low dose CT denoising [20][22-24]. The most popular generative models used for image-to-image translation tasks are autoencoders [24][25], encoder-decoder networks [20][21], fully convolutional neural networks [23][26], and various types of generative adversarial networks (GANs) [22][27].

An autoencoder is an unsupervised neural network that learns how to efficiently compress (encode) data by learning how to reconstruct the data from the compressed (encoded) representation. Encoder-decoder networks are a convolutional version of autoencoders that include connections between encoder and decoder networks. Fully convolutional networks (FCNs) replace the fully connected layer in traditional convolutional neural networks with a deconvolution layer to perform image-to-image translation.

GANs were originally proposed by Goodfellow et al. [27], and have been applied to a variety of image-to-image translation tasks [28][29]. One of the most significative drawbacks of the original GANs is the difficulty to control the output. Mirza et al. [30] proposed conditional GANs (CGANs), which introduced conditional restrictions into GANs to make the output more controllable and training more stable. Yang et al. [22] achieved state-of-art performance in low dose CT denoising using a CGAN with Wasserstein distance and perceptual loss. The main disadvantages of deep learning based methods are the high computational

requirements at training time and the necessity for data collection.

In this article, we focus on using generative models to improve the quality of low dose CT images and assess the impact it has on the reproducibility of radiomic features. Source code of the whole project with good ReadMe instructions, pre-trained models and supplementary materials will be available at: <https://gitlab.com/UM-CDS/low-dose-ct-denoising/-/branches>, we hope our codes and related documents can help medical scientists to understand and reuse our jobs better.

2. Methods and Materials

Institutional Review Board approval was not applicable for this study, since the primary source of data was an open access collection on The Cancer Imaging Archive (National Institutes of Health) [31] and all patients personal information has been moved from CT scans. This dataset has been used for this study in accordance with the Creative Commons Attribution-NonCommercial 3.0 Unported (CC BY-NC) conditions.

2.1 Model Development

As mentioned in Section 1, FCNs have shown good performance in image-to-image translation tasks, but we excluded them from our experiments because they are unfeasibly slow, since they generate new images pixel-by-pixel. Being a convolutional version of autoencoders, encoder-decoder networks should have a better performance for image-to-image translation tasks [21]. Therefore, we excluded autoencoders from our experiments in favour of encoder-decoder networks. CGANs were also included in the experiments for their proven performance in low dose CT denoising [22].

The architecture of the encoder-decoder network is shown in Figure 1. It is a 5-layer network consisting of 32 (3×3)-sized convolution and deconvolution kernels with padding to keep the image size constant after each convolution or deconvolution. Max pooling layers are used with 2×2 size filters and a stride of 2. We used cross entropy loss as the loss function in our network and leaky rectified linear units (LReLUs) as activation functions. The original 512×512×1 CT matrix was used as the size of input and output images in training and testing.

For the CGAN, we follow the same architectures and parameter settings proposed in [30][32]. The architecture of the CGAN is illustrated in Figure 2. We adjusted the networks' input and output sizes from the original size to 512×512×1. Finally, we adjusted the networks to output DICOM files directly for better radiomic feature calculation. The loss function of CGAN were set as cross entropy loss too.

In order to compare the performance of generative models with that of traditional denoising methods, we included a low-

pass filter – non-local means algorithm [33] – as representative for traditional denoising methods. There are several reasons support us to choose non-local means algorithm as our testing traditional denoising method. First of all, non-local matching based denoising method received the better performance by comparing with other traditional methods [34]. Secondly, non-local means algorithm running faster than other non-local matching based algorithms and receive similarly denoising result such as Block-Matching and 3D filtering (BM3D) [34][35]. For the non-local means algorithm, we set the size of the ‘search windows’ to 5 and the filtering parameter h to 7.

2.2 Model Development

We used the NSCLC-Radiomics dataset [36] (hereafter called LUNG 1), which contains CT scans of 422 non-small cell lung cancer (NSCLC) patients, as our experimental dataset. These CT scans include outlines drawn by professional radiation oncologists that delineate a region of interest (ROI), i.e. the tumor volume. Tumor delineations are necessary to be able to calculate radiomic features. The CT images for which the dose level (‘parameter exposure’ in DICOM metadata) is missing ($n=200$) were excluded from the analyses. We considered CT images scanned at 400 milliampere-seconds (mAs) and above as full dose CT ($n=157$, the index of LUNG 1 patients included in the experiments can be found in Supplementary Table 1, supplementary materials are available: <https://gitlab.com/UM-CDS/low-dose-ct-denoising/-/branches>). These data were be used for training ($n=40$, 4260 frames) and testing ($n=117$, 13423 frames). Conversely, we designated CT images scanned with 50 mAs as low dose CT, following the definition from the Low Dose CT Grand Challenge[21][37].

As already mentioned, training encoder-decoder networks and CGANs requires paired images, in our case, pairs of matching low dose and full dose CT scans. Since LUNG 1 has no paired images, we simulated the noisy degradation present in low dose CT images by introducing noise based on the method proposed in literature [21][37]. In these articles, the authors mimicked CT scanners’ behavior by adding noise with a normal distribution into a sinogram (by Radon transform) and reconstructed the CT image from the modified sinogram to obtain simulated noisy images. We used a similar method to add noise in the original sinogram as follows:

$$z_i = (1 + b_i)e^i + r_i, i = 1, \dots, I, b_i \sim N(\mu, \sigma) \quad (1)$$

where z_i is the measurement along the i -th ray path; r_i is the read-out error; e^i represents the original line integral of attenuation coefficients along the i -th ray path; and, b_i is the black scanner factor, which follows a normal distribution. The intensity of noise added to the image can be controlled through the parameter b_i .

In order to mimic low dose CT images (scanned with 50mAs) from full dose CT images (scanned with 400 mAs),

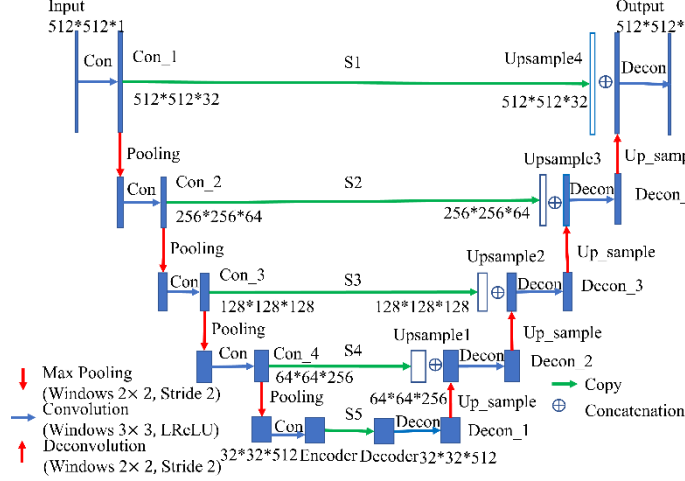


Figure 1. The architecture of the encoder-decoder network we first measured the noise intensity introduced in images with lower doses by scanning a Gammex 467 CT phantom (Middleton, WI, USA) using a Philips Brilliance Big Bore CT with different doses (400 mAs, 50 mAs) [38]. The signal-to-noise ratio (SNR) of the real phantom dataset is 19.7 dB (95%CI [17.8, 21.6]). We estimated that a σ of 0.0035 mimicked best the noise in 50 mAs CT images from 400 mAs image (referred to as low-noise images hereafter). The SNR of simulated low-noise images is 18.3 (95%CI, [16.9, 20.1]) dB. In order to assess the reproducibility of radiomic features with noise of different intensities, we added stronger noise (25 times noise power) as mentioned above to the full dose CT (400 mAs), setting σ to 0.0068 to mimic CT images with stronger noise (referred to as high-noise images hereafter). The SNR of simulated high-noise images is 6.0 (95%CI, [5.9, 6.1]) dB. Additionally, the external noise introduced by Radon transform and inverse Radon transform was removed from the generated images. A comparison of noise in simulated image and in real phantom dataset is shown in Figure 3, the intensity of noise in real phantom is 17.1 dB and average noise power spectra density within whole image is 45.8 W/Hz. The intensity of noise in simulated low-noise images is 19.4 dB and average noise power spectra density within whole image is 3.6 W/Hz, intensity of noise in simulated high-noise images is 6.1 dB and average noise power spectra density within whole image is 6.0 W/Hz.

We used 40 subjects from LUNG 1 (4260 images in total) for training in all three models and 117 subjects from LUNG 1 for testing. Training was only based on paired low dose (high-noise) and full dose images for all models. Denoising for low-noise images was performed using pretrained models without retraining.

Moreover, in order to test the performance of our models in denoising real low dose CT, we used two additional datasets. First, a collection of phantoms CTs scanned at different exposure levels [38]. Second, the Reference Image Database to Evaluate Therapy Response (RIDER), a collection of same-day repeat CT scans collected to assess the variability of tumor

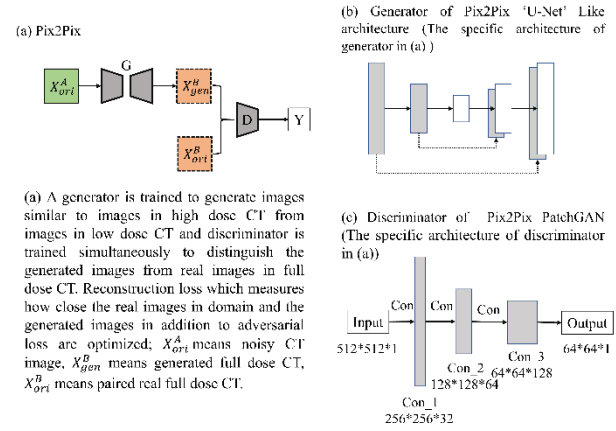


Figure 2. The architecture of the CGAN (Pix2Pix) measurements [39]. This dataset contains CT scan pairs for 32 NSCLC patients with corresponding segmentation masks. These CT images were scanned at low dose (7 to 13 mAs), making it suitable for our denoising experiment.

2.3 Calculation of Radiomic Features

All images were loaded and analysed (i.e. radiomic feature extraction) using the O-RAW open source software [40]. Radiomic features are divided in three groups – shape features, intensity histogram (first-order) features and textural (Haralick) features. In our experiments, the masks for calculating radiomic features are not affected by denoising, and therefore shape features were excluded from further analysis. Finally, 90 radiomic features (listed in Supplementary Table2, supplementary materials are available: <https://gitlab.com/UM-CDS/low-dose-ct-denoising/-/branches>) were included in our analyses.

2.4 Experiments

All experiments were executed in an Amazon EC2 G3 Graphics Accelerated Instance with a Tesla M60 GPU, 30.5GB of memory and 4 CPUs.

We executed three kinds of experiments using the test set from LUNG 1 to assess how denoising CT images using different types of generative models (encoder-decoder, CGAN) and one traditional denoising algorithm (non-local means), different numbers of training epochs (25, 50, 75 and 100) and different noise intensities (low and high noise images) affects the reproducibility of radiomic features. We compared feature reproducibility of radiomic features in noisy CTs to reproducibility in denoised CT scans, by calculating the correlation of each radiomic feature between each full dose CT image and their respective noisy/denoised CT scan. In order to assess the impact of denoising on real low dose CT scans using the models trained on LUNG 1, we ran two additional experiments. First, we used the models trained on LUNG 1 to denoise low dose CT scans of phantoms (50 mAs

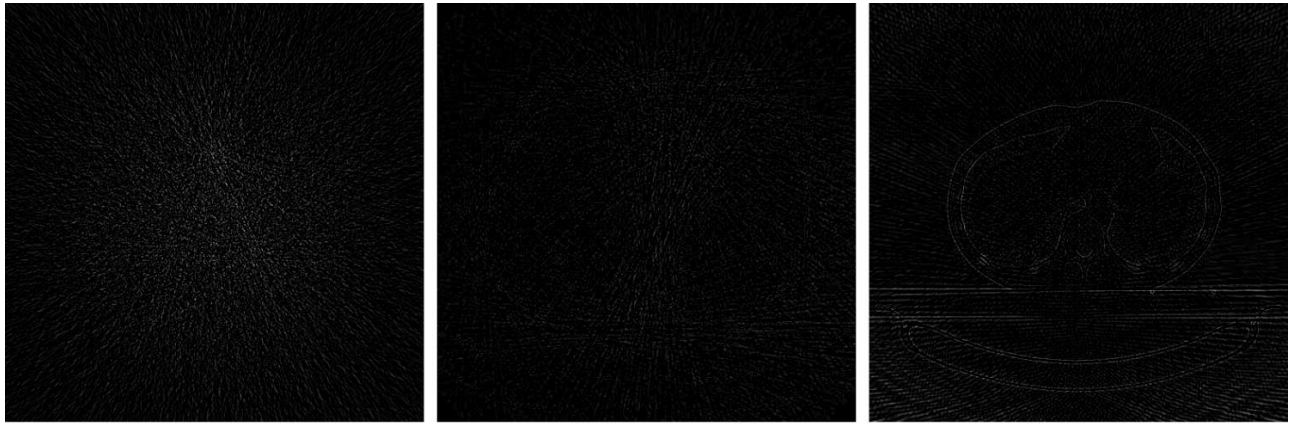


Figure 3. A comparison of noise in simulated images and in a real phantom image. (a) real phantom image; (b) simulated low-noise image; (c) simulated high-noise image.

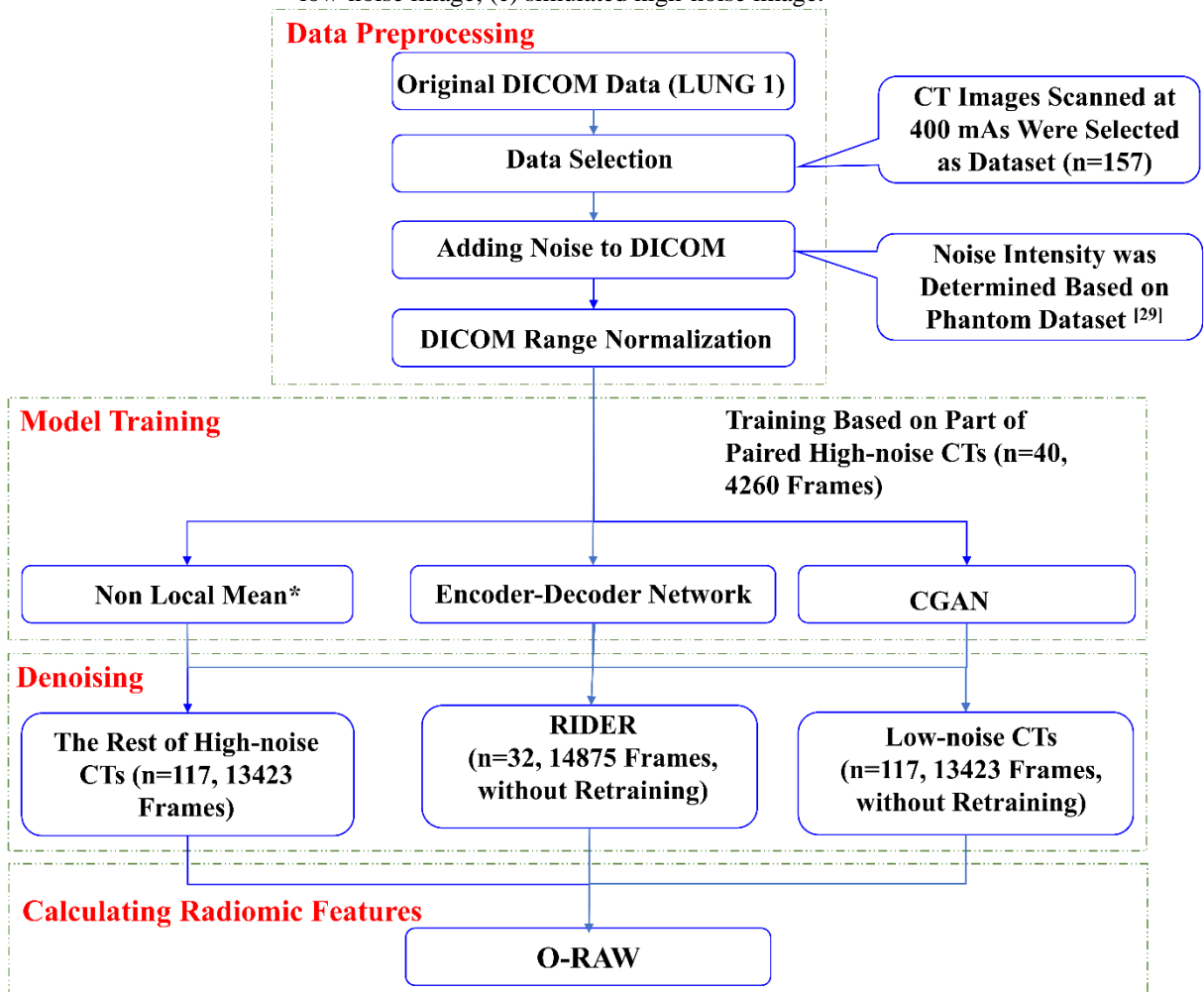


Figure 4. Flowchart of methods. *Non-local means algorithm applied only on The Rest of High-noise CTs and Low-noise CTs datasets.

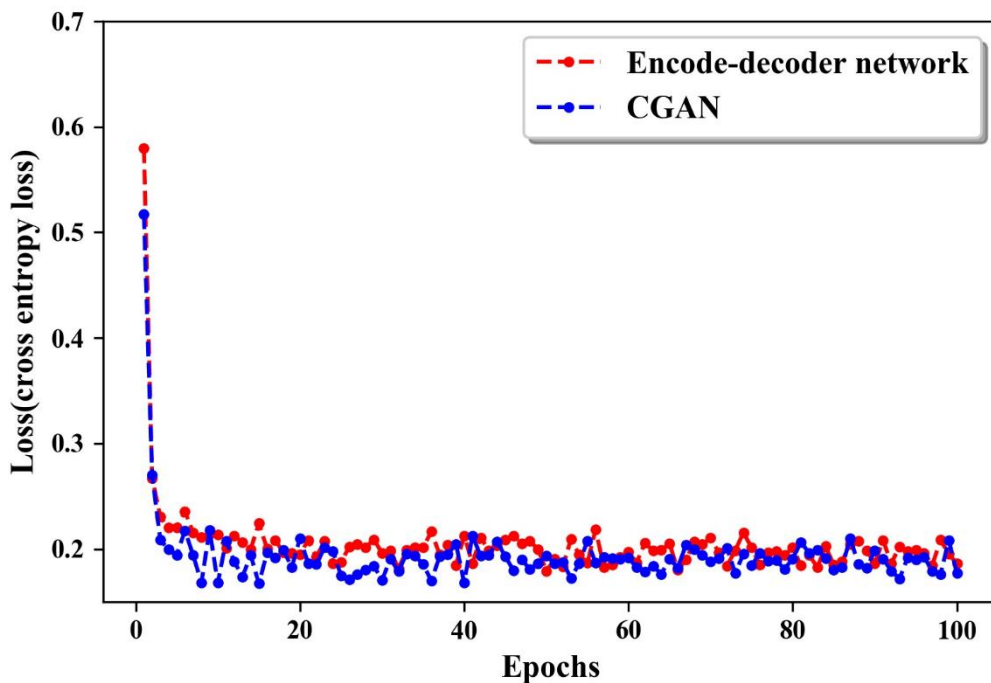


Figure 5. Loss function (cross entropy loss) curves of encoder-decoder network and CGAN along with different training epochs

equivalent to simulated low dose CT scans) and compared the difference between low and full dose CT to the difference between denoised and full dose CT. Second, we ran an experiment to assess the impact of denoising on the test-retest reliability of radiomic features using the RIDER dataset, which contains same day CT scan pairs of patients with NSCLC. Finally, we compared the test-retest reliability of radiomic features in original versus denoised CT scans by calculating the correlation between the CT scan pairs for each radiomic feature.

2.5 Statistical Analysis

Correlation was measured using the concordance correlation coefficient (CCC), as defined in [41]. In addition, we measured the difference between the original full dose CT images and denoised images using Root Mean Square Error (RMSE) and content loss [42]. Content loss was calculated based on a pretrained VGG-16 [43].

The definition of RMSE is shown in equation (2):

$$RMSE = \sqrt{\frac{1}{M} \sum_{i=1}^M (y_i - \hat{y}_i)^2} \quad (2)$$

Where y_i and \hat{y}_i represent the image value in position i for original full dose CT and denoised CT respectively, moreover, image y and \hat{y} are normalized to 0-1 before calculating RMSE. M represents number of pixels in one image and it is 512*512 in our case.

The flowchart summarizing our study methodology is shown in Figure 4.

3. Results

Training took 8 hours and 20 hours for the encoder-decoder network and the CGAN respectively. The loss function (cross entropy loss) curves of encoder-decoder network and CGAN along with different training epochs are shown in Figure 5. The trained models were used to generate denoised CT scans of the test set. An example of an original, noisy and denoised CT scan is shown in Figure 6 (corresponding figure for high-noise images is shown in Supplementary Figure 1). Moreover, Table 1 shows the RMSE, content loss and ratio of poor, medium, and good reproducibility radiomic features. Following the classification in [8], the reproducibility of a feature is good, medium or poor when the CCC ≥ 0.85 , $0.65 \leq CCC < 0.85$ and $CCC < 0.65$ respectively). We summarize the reproducibility of radiomic features in low-noise images and their denoised counterparts using a heatmap in Figure 7 (corresponding figure for high-noise images is shown in Supplementary Figure 2, the CCCs for each feature in different models can be found in Supplementary Tables 3-4).

3.1 Effect of Different Models

As shown in Table 1, the baseline RMSE and content loss of high-noise and low-noise images (before denoising) were 0.0237/0.0781 (RMSE/content loss) and 0.0225/0.0706 respectively. The RMSE and content loss were decreased to 0.0175/0.0443 for high-noise images and 0.0173/0.0427 for

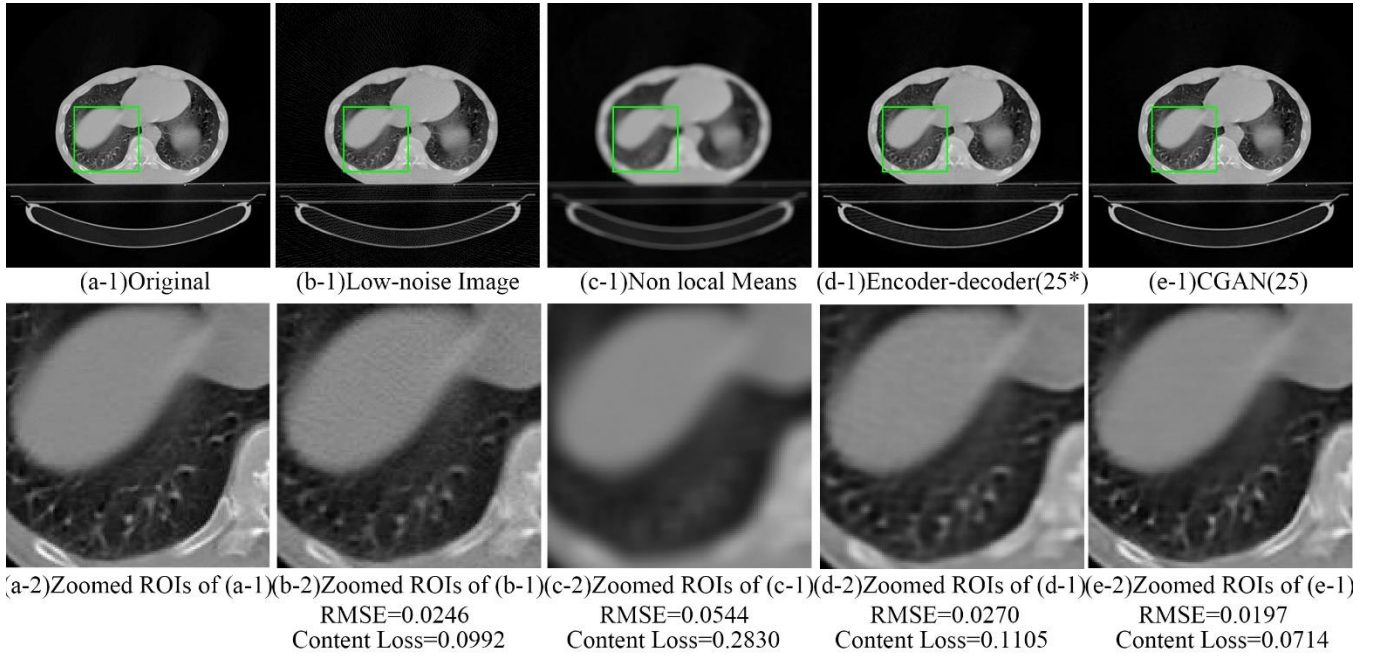


Figure 6. Example of low dose CT denoising. (a-1) The original full dose CT image; (b-1) Low-noise image; (c-1) Image denoised using non-local means; (d-1) Image denoised by encoder-decoder network (Training at 25 epochs); (e-1) Image denoised by CGAN; (a-2) to (e-2) Zoomed ROIs for (a-1) to (e-1). We regard the higher noise in (d-2) by comparing with (b-2) as a coincidence.

Table 1. Summary of RMSE, content loss and distribution of CCCs of radiomic features

Models \ Distribution	RMSE	Content loss	CCCs<0.65	0.65≤CCCs<0.8 5	CCCs≥0.85
Low-noise Images					
Without denoising	0.0225	0.0706	0/17(0%)* 9/73(12%)** 9/90(10%)***	3/17(18%) 17/73(24%) 20/90(22%)	14/17(82%) 47/73(64%) 61/90(68%)
Non-Local Means	0.0993	0.3280	5/17(29%) 48/73(66%) 53/90(59%)	8/17(47%) 21/73(29%) 29/90(32%)	4/17(24%) 4/73(5%) 8/90(9%)
			0/17(0%) 0/73(0%) 0/90(0%)	1/17(6%) 16/73(22%) 17/90(19%)	16/17(94%) 57/73(78%) 73/90(81%)
			0/17(0%) 3/73(4%) 3/90(3%)	0/17(0%) 15/73(21%) 15/90(17%)	17/17(100%) 55/73(75%) 72/90(80%)
High-noise Images					
Without denoising	0.0237	0.0781	5/17(29%)	1/17(6%)	11/17(65%)

		27/73(37%)	20/73(27%)	26/73(36%)
		32/90(36%)	21/90(23%)	37/90(41%)
Non-Local Means	0.1095 0.3941	6/17(35%)	7/17(41%)	4/17(24%)
		52/73(71%)	17/73(23%)	4/73(6%)
		58/90(64%)	24/90(27%)	8/90(9%)
Encoder-decoder	0.0175 0.0443	0/17(0%)	1/17(6%)	16/17(94%)
		4/73(5%)	13/73(18%)	56/73(77%)
		4/90(4%)	14/90(16%)	72/90(80%)
CGAN	0.0146 0.0305	0/17(0%)	1/17(6%)	16/17(94%)
		0/73(0%)	13/73(18%)	60/73(82%)
		0/90(0%)	14/90(16%)	76/90(84%)

* represents the summary of fist order features; ** represents the summary of textural features; *** represents the summary of all features.

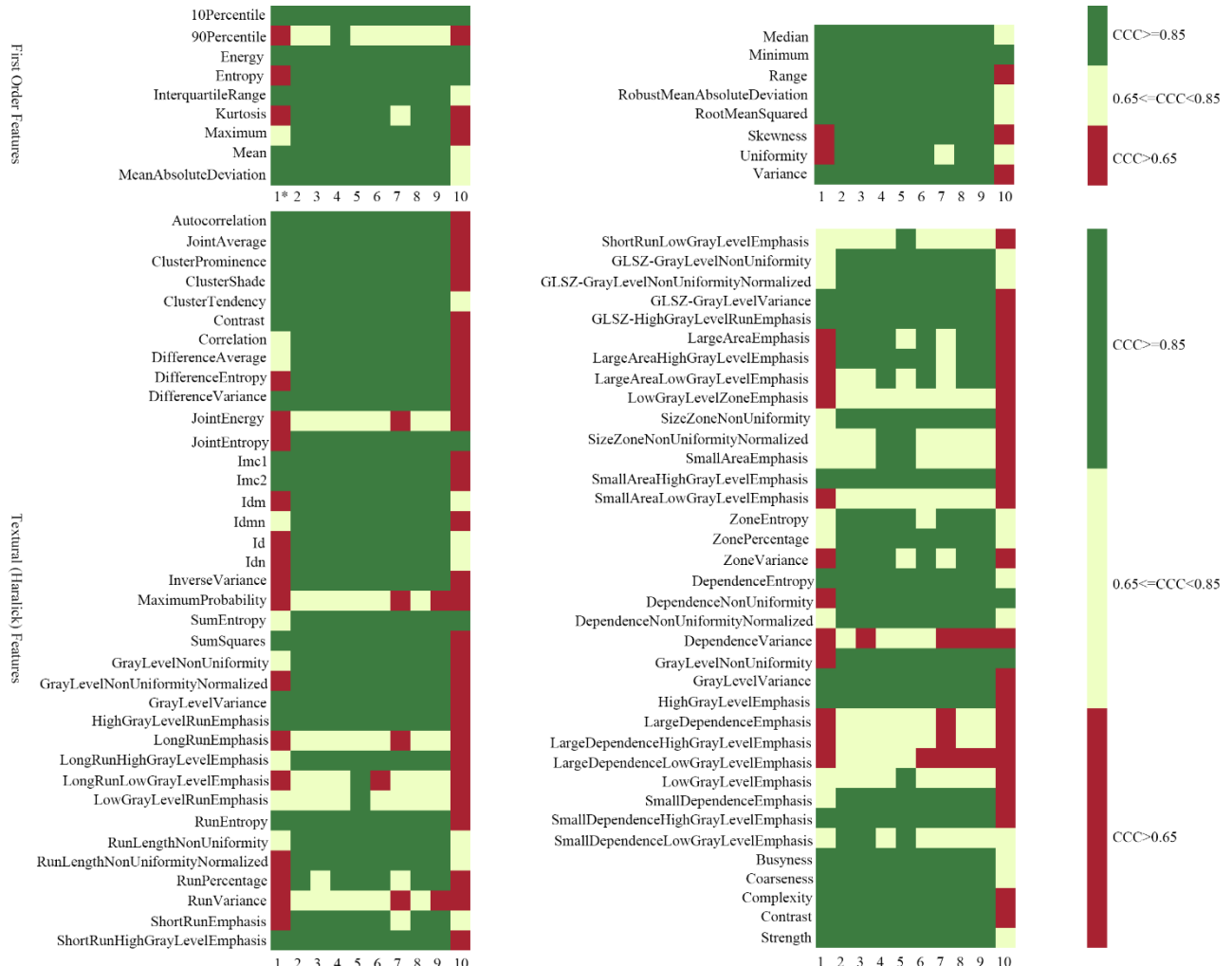


Figure 7. Heatmap of radiomic features' reproducibility based on high-noise/denoised images. *1 represents CCC of radiomic features calculated based on high-noise images; 2-5 represent CCC of radiomic features calculated based on

denoised images by using CGAN when network trained at 25, 50, 75, 100 epochs; 6-9 represent CCC of radiomic features calculated based on denoised images by using encoder-decoder network when network trained for 25, 50, 75, 100 epochs respectively; 10 represent CCC of radiomic features calculated based on denoised images by using non-local means algorithm.

low-noise images, respectively by using encoder-decoder network. On the other hand, RMSE and content loss were decreased to 0.0146/0.0305 and 0.0143/0.0290 by using CGAN. As shown in Figure 8, the baseline CCC means of high-noise and low-noise images were 0.681 and 0.867. In contrast, the means of the CCC for denoised images using the encoder-decoder network and the CGAN (trained for 100 epochs) were around 0.92, both for high-noise and low-noise images. In comparison, RMSE and content loss were increased to 0.1095/0.3941 and 0.0993/0.3280 by non-local means algorithm; the CCC means of images denoised using the non-local means algorithm were 0.525 and 0.555 for high-noise and low-noise images, respectively. The cumulative distribution function of CCCs for different models when trained for 100 epochs is shown in Figure 8. The encoder-decoder network and the CGAN improved the reproducibility of radiomic features significantly, especially for the high-noise images. Non-local means algorithm can remove noise from image as we can see in Figure 6 (c-1). However, it also removed the details of images, as shown in Figure 6 (c-2), a phenomenon referred to as smoothing in the literature. [5] In other words, the smoothing from a special low-pass noise filter caused a deterioration in radiomics reproducibility in terms of CCC (Wilcoxon signed-rank test, p-value <0.01).

3.2 Effect of Different Numbers of Training Epochs

An example of an original, noisy and denoised CT scan at different training epochs by using encoder-decoder network and CGAN is shown in Figure 9. The cumulative distribution function of the CCCs of radiomic features on images denoised with the CGAN trained for different numbers of epochs is shown in Figure 10. As shown in the graph, the best results in low-noise images were achieved when the CGAN was trained for 25 epochs. However, there is no significant difference in high-noise images. This phenomenon can also be found in encoder-decoder network (Supplementary Figure 3), where the results were worst when trained for 50 epochs. We speculate that this phenomenon is a result of coincidence, an artefact of training convergence, rather than a meaningful finding. In addition, we show the RMSE, content loss of images and ratio of poor, medium, and good reproducibility radiomic features denoised with the CGAN when it was trained for different numbers of epochs in Table 2 (corresponding Tables for the encoder-decoder network can be found in Supplementary Table 5). The RMSE and content loss in the whole dataset for images denoised using CGANs trained for different numbers of epochs are shown in Table 2.

3.3 Effect of Different Noise Intensities

As mentioned in Section 2, the models were not retrained for denoising low-noise images. Figure 11 shows the cumulative distribution functions of CCCs of radiomic features calculated from images to which different levels of noise intensity were applied. We compared the CCC distributions of radiomic features calculated on images denoised from high-noise images with those of images denoised from low-noise images using the Wilcoxon signed-rank test. The p-value for the CGAN, the encoder-decoder network are 0.671 and 0.109 respectively. These results imply that CGANs and encoder-decoder networks trained to denoise high-noise images can be applied to denoise images with different levels of noise and achieve similar results. In other words, a single pretrained model can be used to improve the reproducibility of radiomic features in images with different levels of noise intensity, especially when the dose of the image is lower than 50 mAs.

3.4 Effect in real low dose CT scans

In order to test the denoising performance in real low dose CT scans, we ran two different experiments. First, we used trained models to denoise low dose CT scans of phantoms and compared them to their respective full dose CT scans. The RMSEs of denoised versus full dose CT scans using the encoder-decoder network and CGAN were 0.0182 and 0.0140 respectively, compared with 0.0231 in the original low dose CTs. The content loss in CT scans denoised using the encoder-decoder network and CGAN was 0.0433 and 0.0289, compared with 0.0702 in the original low dose CTs. Second, we assessed the effect of denoising on the test-retest reliability of radiomic features using the RIDER dataset. In light of the poor performance of the cycle GAN in previous experiments, it was excluded from this experiment. The results in Table 3 show that denoising using the encoder-decoder network and the CGAN improved the mean CCCs of radiomic features from 0.90 to around 0.94, and the percentage of features with a CCC higher than 0.85 increased from 80% to around 90%. The cumulative distribution of CCCs for radiomic features can be found in Figure 12. We can therefore conclude that these models can improve the test-retest reliability of radiomic features calculated from low dose CT scans.

4. Discussion

Our objective was to test three different deep learning generative models to improve the signal-to-noise in CT images and examine the effect of denoising on radiomic features

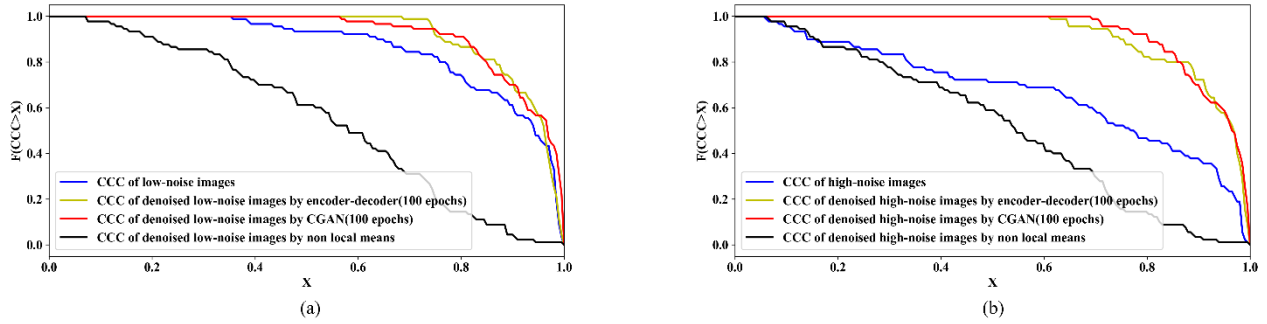


Figure 8. Cumulative distribution function of CCC by using different models. (a) Cumulative distribution function of CCC based on denoised low-noise images by using different models; (b) Cumulative distribution function of CCC based on denoised high-noise images by using different models.

Table 2. RMSE, content loss and ratio of poor, medium, and good reproducibility radiomic features for images denoised by the CGAN trained for different numbers of epochs

Training length \ Noisy images	25 Epochs	50 Epochs	75 Epochs	100 Epochs
Low-noise Images				
RMSE	0.0148	0.0144	0.0142	0.0143
Content loss	0.0295	0.0290	0.0276	0.0290
CCCs ≥ 0.85	81/90(90%)	73/90(81%)	70/90(78%)	72/90(80%)
$0.65 \leq \text{CCCs} < 0.85$	9/90(10%)	17/90(19%)	18/90(20%)	15/90(17%)
CCCs < 0.65	0/90(0%)	0/90(0%)	2/90(2%)	3/90(3%)
High-noise Images				
RMSE	0.0150	0.0148	0.0144	0.0146
Content loss	0.0309	0.0312	0.0291	0.0305
CCCs > 0.85	72/90(80%)	71/90(79%)	75/90(83%)	76/90(84%)
$0.65 \leq \text{CCCs} < 0.85$	18/90(20%)	18/90(20%)	15/90(17%)	14/90(16%)
CCCs < 0.65	0/90(0%)	1/90(1%)	0/90(0%)	0/90(0%)

Table 3. Effect of denoising on test-retest reliability of radiomic features

Epochs \ CCCs > 0.85	25 Epochs	50 Epochs	75 Epochs	100 Epochs	Original RIDER
Encoder-decoder	78/90(0.923*)	82/90(0.936)	78/90(0.925)	78/90(0.906)	72/90(0.897)
CGAN	81/90(0.928)	81/90(0.920)	85/90(0.939)	83/90(0.929)	

*Mean CCCs of radiomic features.

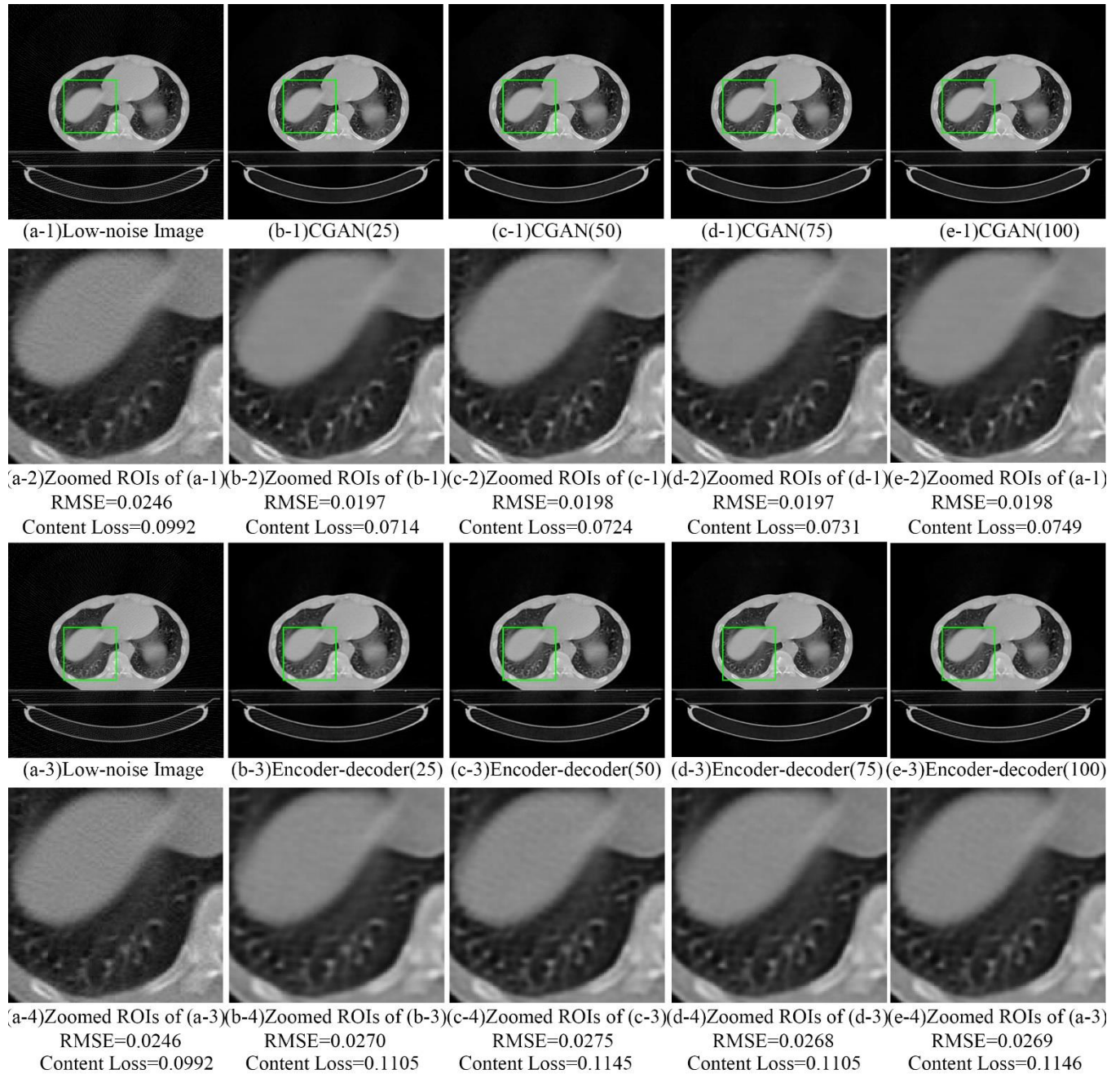


Figure 9. An example of an original, noisy and denoised CT scan at different training epochs by using the encoder-decoder network and the CGAN. As we can see figures (b-4) to (e-4), the RMSE and content loss of denoised images is higher in this particular case than the original low-noise images.

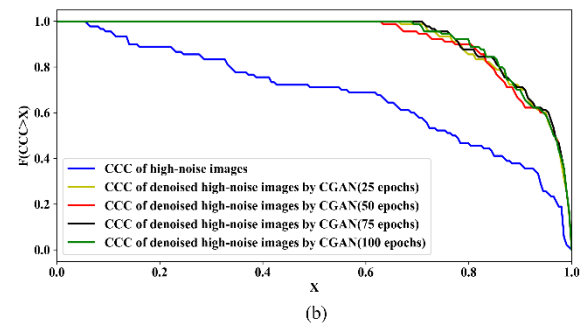
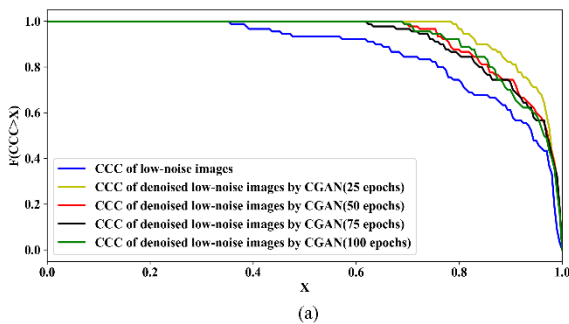


Figure 10. Cumulative distribution function of CCCs for image denoised by CGAN trained for different numbers of epochs. (a) Cumulative distribution function of CCCs based on denoised low-noise by using CGAN trained for different numbers of epochs; (b) Cumulative distribution function of CCCs based on denoised high-noise by using CGAN trained for different numbers of epochs.

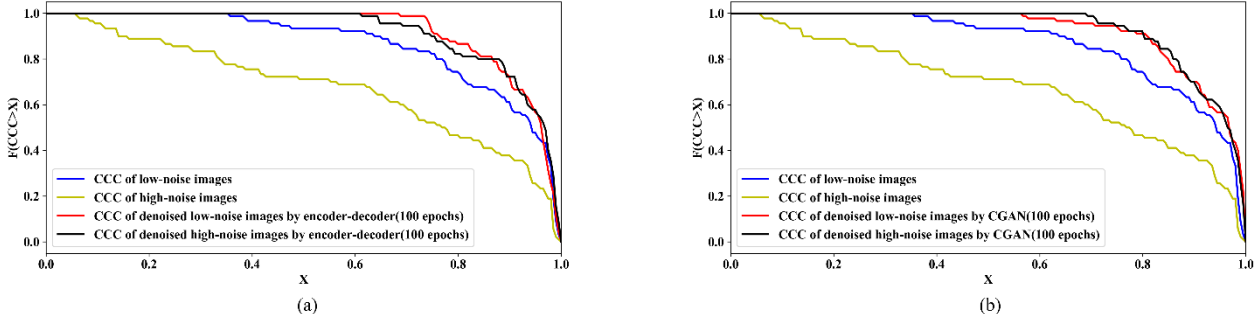


Figure 11. Cumulative distribution functions of CCCs for image noised with different intensities. (a) Cumulative distribution functions of CCCs for image noised with different intensities (Encoder-decoder network); (b) Cumulative distribution functions of CCCs for image noised with different intensities (CGAN).

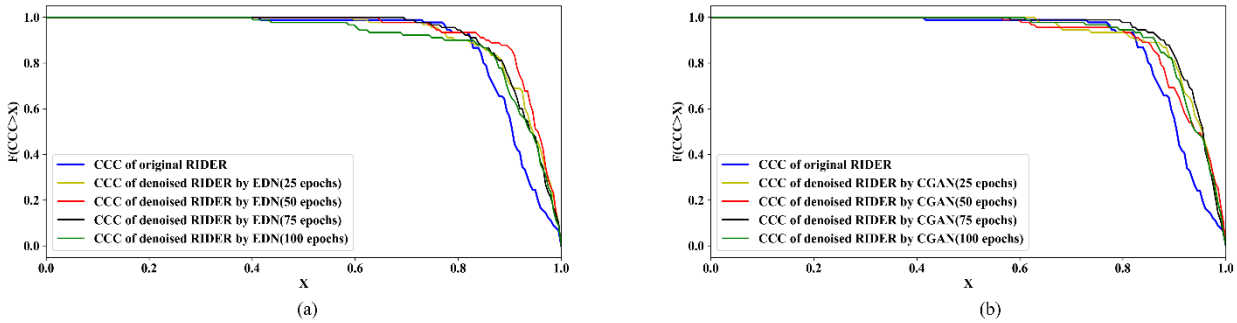


Figure 12. Cumulative distribution functions of CCCs for original and denoised CT scans in the RIDER dataset (a) using a CGAN trained for different numbers of epochs; (b) using an encoder-decoder network trained for different numbers of epochs

reproducibility. The results of our experiments show that an equivalent good performance, in terms of reducing RMSE and content loss and increasing the CCC of radiomic features, was obtained by CGANs and encoder-decoder networks. On the other hand, the poor performance of non-local means algorithm probably roots from the low ability of algorithm to keep image details during denoising by comparing with CGANs and encoder-decoder networks, this point can be found in Figure 6.

The improvement in radiomic feature reproducibility using denoising in low dose CT scans (≤ 50 mAs) has been tested and reported above. However, it is worth testing if our generative models can perform equally well on a wider range of scanners and scanning conditions. The results from low-noise images indicate that the denoising models generalize to images with different characteristics, but more varying scanning and reconstruction characteristics are needed to confirm this. If so, this will reduce applicability barriers for clinicians and radiomics practitioners significantly.

The main limitations of this study are that the training data are not real paired low/full dose CT images due to the difficulty of collecting such paired images. However, we

showed in our experiments that denoising has a beneficial impact on real low dose CT scans in terms of radiomics reproducibility. Secondly, we spent limited time fine-tuning the hyperparameters of the models. Therefore, the results shown in our experiments may not be the best results achievable with the experimental models, especially for cycle GANs. Third, we transformed DICOM images to PNG images to use them as the input to the networks. This transformation will result in loss of information due to rounding errors. Fourth, our training data originates from a single center. The robustness and generalizability of our models needs to be tested using data from multiple centers. Fifth, the cost functions used to train the generative models may not be the best to optimize the radiomic features' CCC due to the absent of comparative experiments on other cost functions. Sixth, it will be better if more quantitative metrics can be provided to evaluate the goodness of the generative model based approaches, only RMSE, content loss and CCC were included in this article, this point may introduce the phenomenon of worse image quality after denoising by using encoder-decoder network as shown in Figure 9. Finally, we did not show a direct benefit in any application of radiomics, such as increased performance of a

prediction model. This is beyond the scope of this article but we argue that reproducibility of radiomic features in itself is likely to improve the robustness of any potential application of radiomics.

Future work might further improve the reproducibility of radiomics. For example, the mask used to calculate radiomic features was drawn by a clinician on full dose CT images. However, the masks might have been different if they had been drawn based on noisy images, such as low dose CT scans. Therefore, a noise insensitive tumor segmentation algorithm could potentially improve low dose CT radiomic feature calculation.

For future studies radiomics studies and radiomics feature reproducibility, we will make source code of our whole project with good ReadMe instructions, pre-trained models and supplementary materials available at: <https://gitlab.com/UM-CDS/low-dose-ct-denoising/-/branches>.

5. Conclusion

In this article, we have analyzed the performance of one traditional denoising method – non-local means algorithm – and two different deep learning generative models – encoder-decoder networks, CGANs – to improve the reproducibility of radiomic features calculated from noisy images such as low dose CT scans. We added noise of two intensities —weak noise and strong noise— to full dose CT images. All models were trained using high-noise images, and high and low-noise images were denoised using these models, without retraining. The results also show that the non-local means algorithm decreases the reproducibility of radiomic features. Moreover, encoder-decoder networks and CGANs can improve the reproducibility of radiomics. In addition, the results from low-noise images were not significantly different to those of high-noise images. These results imply that images with varying levels of noise can be denoised using our trained models to improve the reproducibility of radiomic features, as long as the noise is equal or higher than that in images with a dose lower than 50 mAs. To the authors' best knowledge, this article is the first to show an improvement in the reproducibility of radiomics based on low dose CT denoising.

Acknowledgements

J Chen is supported by a China Scholarship Council scholarship (201906540036) and a YERUN Research Mobility Award. The remaining authors acknowledge funding support from the following: STRaTegy (STW 14930), BIONIC (NWO 629.002.205), TRAIN (NWO 629.002.212), CARRIER (NWO 628.011.212) and a personal research grant by The Hanarth Funds Foundation for L Wee.

References

[1] Lambin, Philippe, et al. "Radiomics: the bridge

between medical imaging and personalized medicine." *Nature reviews Clinical oncology* 14.12 (2017): 749.

- [2] Desseroit, Marie-Charlotte, et al. "Reliability of PET/CT shape and heterogeneity features in functional and morphologic components of non-small cell lung cancer tumors: a repeatability analysis in a prospective multicenter cohort." *Journal of Nuclear Medicine* 58.3 (2017): 406-411.
- [3] Bogowicz, Marta, et al. "Stability of radiomic features in CT perfusion maps." *Physics in Medicine & Biology* 61.24 (2016): 8736.
- [4] Tixier, Florent, et al. "Reproducibility of tumor uptake heterogeneity characterization through textural feature analysis in 18F-FDG PET." *Journal of Nuclear Medicine* 53.5 (2012): 693-700.
- [5] Bagher-Ebadian, Hassan, et al. "On the impact of smoothing and noise on robustness of CT and CBCT radiomic features for patients with head and neck cancers." *Medical physics* 44.5 (2017): 1755-1770.
- [6] Aerts, Hugo JWJL, et al. "Decoding tumour phenotype by noninvasive imaging using a quantitative radiomics approach." *Nature communications* 5.1 (2014): 1-9.
- [7] Traverso, Alberto, et al. "Repeatability and reproducibility of radiomic features: a systematic review." *International Journal of Radiation Oncology* Biology* Physics* 102.4 (2018): 1143-1158.
- [8] van Timmeren, Janna E., et al. "Test-retest data for radiomic feature stability analysis: generalizable or study-specific?." *Tomography* 2.4 (2016): 361.
- [9] Huang, Qiao, et al. "Interobserver variability in tumor contouring affects the use of radiomics to predict mutational status." *Journal of Medical Imaging* 5.1 (2017): 011005.
- [10] Musolino, Stephen V., Joseph DeFranco, and Richard Schlueck. "The ALARA principle in the context of a radiological or nuclear emergency." *Health physics* 94.2 (2008): 109-111.
- [11] Sharma, Abhishek, and Vijayshri Chaurasia. "A review on magnetic resonance images denoising techniques." *Machine Intelligence and Signal Analysis*. Springer, Singapore, 2019. 707-715.
- [12] Kollem, Sreedhar, Katta Rama Linga Reddy, and Duggirala Srinivasa Rao. "A Review of Image Denoising and Segmentation Methods Based on Medical Images." *International Journal of Machine Learning and Computing* 9.3 (2019).
- [13] Shan, Hongming, et al. "3-D convolutional encoder-decoder network for low-dose CT via transfer learning from a 2-D trained network." *IEEE transactions on medical imaging* 37.6 (2018): 1522-

1534.

[14] Chen, Hu, et al. "Low-dose CT with a residual encoder-decoder convolutional neural network." *IEEE transactions on medical imaging* 36.12 (2017): 2524-2535.

[15] Yang, Qingsong, et al. "Low-dose CT image denoising using a generative adversarial network with Wasserstein distance and perceptual loss." *IEEE transactions on medical imaging* 37.6 (2018): 1348-1357.

[16] Kang, Eunhee, et al. "Deep convolutional framelet denoising for low-dose CT via wavelet residual network." *IEEE transactions on medical imaging* 37.6 (2018): 1358-1369.

[17] Fan, Fenglei, et al. "Quadratic Autoencoder (Q-AE) for Low-dose CT Denoising." *IEEE Transactions on Medical Imaging* (2019).

[18] Xu, Wenju, Shawn Keshmiri, and Guanghui Wang. "Adversarially approximated autoencoder for image generation and manipulation." *IEEE Transactions on Multimedia* 21.9 (2019): 2387-2396.

[19] Long, Jonathan, Evan Shelhamer, and Trevor Darrell. "Fully convolutional networks for semantic segmentation." *Proceedings of the IEEE conference on computer vision and pattern recognition*. 2015.

[20] Goodfellow, Ian, et al. "Generative adversarial nets." *Advances in neural information processing systems*. 2014.

[21] Yi, Xin, Ekta Walia, and Paul Babyn. "Generative adversarial network in medical imaging: A review." *Medical image analysis* (2019): 101552.

[22] Zhang, Zizhao, Yuanpu Xie, and Lin Yang. "Photographic text-to-image synthesis with a hierarchically-nested adversarial network." *Proceedings of the IEEE Conference on Computer Vision and Pattern Recognition*. 2018.

[23] Mirza, Mehdi, and Simon Osindero. "Conditional generative adversarial nets." *arXiv preprint arXiv:1411.1784* (2014).

[24] Zhu, Jun-Yan, et al. "Unpaired image-to-image translation using cycle-consistent adversarial networks." *Proceedings of the IEEE international conference on computer vision*. 2017.

[25] Isola, Phillip, et al. "Image-to-image translation with conditional adversarial networks." *Proceedings of the IEEE conference on computer vision and pattern recognition*. 2017.

[26] Clark, Kenneth, et al. "The Cancer Imaging Archive (TCIA): maintaining and operating a public information repository." *Journal of digital imaging* 26.6 (2013): 1045-1057.

[27] Aerts, H. J. W. L., Wee, L., Rios Velazquez, E., Leijenaar, R. T. H., Parmar, C., Grossmann, P., ...

Lambin, P. (2019). *Data From NSCLC Radiomics* [Data set]. The Cancer Imaging Archive. <https://doi.org/10.7937/K9/TCIA.2015.PF0M9REI>

[28] McCollough, Cynthia H., et al. "Low-dose CT for the detection and classification of metastatic liver lesions: Results of the 2016 Low Dose CT Grand Challenge." *Medical physics* 44.10 (2017): e339-e352.

[29] Zhovannik, Ivan, et al. "Learning from scanners: Bias reduction and feature correction in radiomics." *Clinical and translational radiation oncology* 19 (2019): 33-38.

[30] Zhao, Binsheng, et al. "Evaluating variability in tumor measurements from same-day repeat CT scans of patients with non-small cell lung cancer." *Radiology* 252.1 (2009): 263-272.

[31] Shi, Zhenwei, et al. "Ontology-guided radiomics analysis workflow (O-RAW)." *Medical Physics* 46.12 (2019): 5677-5684.

[32] Lawrence, I., and Kuei Lin. "A concordance correlation coefficient to evaluate reproducibility." *Biometrics* (1989): 255-268.

[33] Johnson, Justin, Alexandre Alahi, and Li Fei-Fei. "Perceptual losses for real-time style transfer and super-resolution." *European conference on computer vision*. Springer, Cham, 2016.

[34] Simonyan, Karen, and Andrew Zisserman. "Very deep convolutional networks for large-scale image recognition." *arXiv preprint arXiv:1409.1556* (2014).